PHYSICAL REVIEW B VOLUME 2, NUMBER 11 1 DECEMBER 1970

Electron Energy Loss Due to Surface Modes in a Thin Ionic Crystal Film*

J. B. Chase and K. L. Kliewer

Institute for Atomic Research and Development of Physics, Iowa State University, Ames, Iowa 50010

(Received 30 March 1970)

A local theory for the energy loss of a relativistic electron beam, incident normally on a thin ionic crystal film, is developed and applied to the energy region of the surface modes of vibration. It is found that the loss function including retardation is essentially the same as that without retardation. Important effects associated with experimental resolution in energy and momentum are included in the analysis. With the inclusion of the characteristics of the apparatus, the theoretical line shapes and positions are in good agreement with the experimental results on LiF obtained by Boersch, Geiger, and Stickel. A study of the effects of substrate thickness and conductivity is reported. A good conductor, like aluminum, has a strong effect on the loss function, whereas a poor conductor, like carbon, has little effect.

I. INTRODUCTION

Surface vibrational modes in ionic solids have been the subject of several investigations, both theoretical and experimental. Fuchs and Kliewer[1] predicted the existence of surface modes in LiF and gave their dispersion relations for slabs of arbitrary thickness.

One of the techniques for observing the surface modes is to measure the energy loss experienced by fast electrons projected through a film of the ionic crystal. Some work has been done theoretically to derive energy-loss distribution functions for this case, but these theories have not included the retardation of the electromagnetic fields, or they have not included the effect of the substrate upon which the films are deposited.[2,3] Retardation and substrate effects are of interest because of the experiment of Boersch, Geiger, and Stickel.[4] These investigators measured the energy-loss function for 25-keV electrons normally incident on films of LiF which were deposited on substrates of amorphous carbon and interpreted their measured peak as due to the low-frequency surface mode. Fujiwara and Ohtaka[5] found that their nonretarded single-film theory corroborated this interpretation, and they also showed, in agreement with the experiment, that there should be no loss peak arising from the high-frequency mode. However, their theory did not reproduce the experimental results in any detail.

In this paper, we present a theory of electron energy loss in LiF including retardation[6] and the effects of a substrate. Materials in this theory are represented by a dielectric-response function which is a function of the frequency only, that is, we are considering the local approximation. It is this approximation which FK used in their study of the surface modes of ionic crystals.

Figure 1 shows a regional plot of the K-Ω plane. The dimensionless variables used are

$$K=k/k_t, \tag{1a}$$

$$\Omega=\omega/\omega_t, \tag{1b}$$

$$L=k_t d, \tag{1c}$$

with

$$k_t=\omega_t/c.$$

k is the wave vector, ω is the angular frequency, c is the speed of light, d is the slab thickness, and ω_t is the transverse optical frequency for the ionic crystal. Any transverse wave which has coordinates (K,Ω) putting it on the left-hand side of the light line[7] cannot be entirely mechanical. This wave must couple with a photon field external to the slab and thus is radiative in character. On the other hand, mechanical vibrations which are longitudinal can exist on the left-hand side of

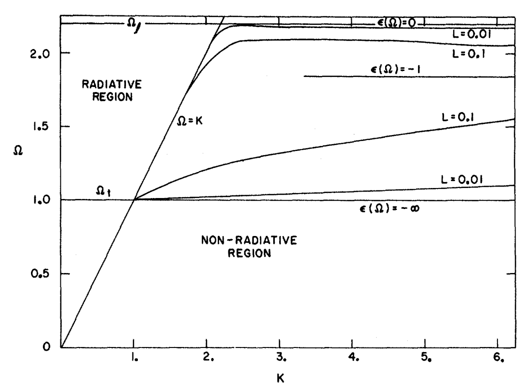

FIG. 1. LiF surface-mode dispersion relations including retardation effects. Curves are plotted for dimensionless slab thicknesses $L=0.01$ ($=520$ Å) and $L=0.1$ ($=5200$ Å).

$K=\Omega$ completely uncoupled from the photons. On the right-hand side of the light line is the nonradiative region. In this region photons can exist coupled to the mechanical waves, but these photons cannot leave the material. In general, as one moves further to the right in Fig. 1, the fraction of the energy in the coupled mechanical-photon waves which is lightlike decreases. So the significance of the light line in this paper is that waves with $K<\Omega$ in general couple to fields outside the slab and can radiate their energy from the material,

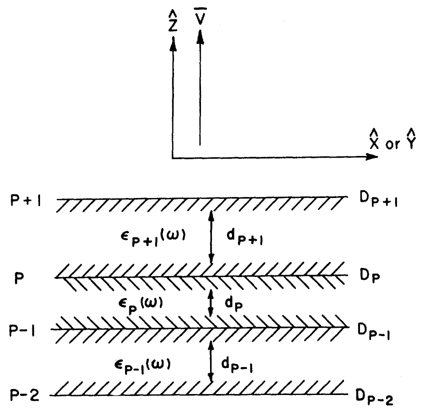

FIG. 2. Multilayer geometry used in the calculation of energy loss for an arbitrary number of layers. The pth layer and the labeling of its boundaries and those of its neighbors are shown explicitly.

whereas energy in waves for which $K>\Omega$ must remain in the material.

FK have shown that in the radiative region there exist normal modes for LiF slabs called virtual modes, and in the nonradiative region there exist polariton and surface modes. Considering Fig. 1 further, we have separated the nonradiative region into three sections in the Ω direction with the lines $\Omega=\Omega_l$ and $\Omega=\Omega_t=1$, the dimensionless longitudinal and transverse optical frequencies defined as the frequencies for which $\epsilon(\Omega)=0$ and $|\epsilon(\Omega)|\rightarrow\infty$, respectively. $\epsilon(\Omega)$ is the local dielectric function of the ionic crystal given by

$$\epsilon(\Omega)=\epsilon_\infty+(\epsilon_0-\epsilon_\infty)/(1-\Omega^2). \tag{2}$$

It is shown in Ref. 1 that for $\Omega>\Omega_l$ and $\Omega<\Omega_t$, on the nonradiative side, there exist a large number of polariton modes which have sinusoidal spacial dependence. The surface modes are found in the region $\Omega_l>\Omega>\Omega_t$ with $\Omega>K$; their amplitudes decrease monotonically as one moves from the surfaces toward the center of the slab. It is the surface modes which are of particular interest in this paper, so on Fig. 1 is plotted, from FK, the dispersion curves for the two surface modes for two thicknesses of LiF.

Because of its longitudinal character, we would anticipate that the electron beam would interact strongly with not only the surface modes but also with the longitudinal modes of the crystal. However, in a thin film these longitudinal modes, all with $\Omega=\Omega_l$, occur only for specific values of the component of the wave vector perpendicular to the film.[1] These restrictive conditions thus preclude striking effects occurring at $\Omega=\Omega_l$ when the film is thin.

In Sec. II the general energy-loss theory for the multilayered slab is developed. Section III is devoted to the analysis of the computed energy-loss function for a LiF slab with and without a substrate and the comparison of the results of these calculations with the experimental data of BGS. Conclusions drawn from this work are given in Sec. IV along with suggestions for future theoretical and experimental work in this area.

II. ENERGY-LOSS FUNCTION FOR "$l-1$" ADJACENT FILMS

The energy loss is obtained by calculating the total work done on the incident particle by the fields induced in the slab by the particle. In determining the fields we consider the incident particle as not deviating from its initial velocity which limits the theory to high-energy electrons. Changes in the velocity of the particle are higher-order effects.

It is necessary to calculate the total electric field in the presence of the incident charge for $l-1$ slabs bounded by l surfaces using the geometry shown in Fig. 2. We express the current associated with the incident charge as

$$\mathbf{J}(\mathbf{x},t)=e\hat{z}v\delta(x)\delta(y)\delta(z-vt),$$

where v is the velocity of the particle, $\mathbf{x}$ is its positive, e is its charge, t is the time, and $\hat{x}$, $\hat{y}$, and $\hat{z}$ are unit vectors in the respective Cartesian directions. Assuming nonmagnetic media, Maxwell's equations are

$$\begin{aligned}
\nabla\times\mathbf{E}(\mathbf{x},t)&=-(1/c)(\partial/\partial t)\mathbf{B}(\mathbf{x},t),\\
\nabla\times\mathbf{B}(\mathbf{x},t)&=(1/c)(\partial/\partial t)\mathbf{D}(\mathbf{x},t)+(4\pi/c)\mathbf{J}(\mathbf{x},t),\\
\nabla\cdot\mathbf{D}(\mathbf{x},t)&=4\pi\rho(\mathbf{x},t),\\
\nabla\cdot\mathbf{B}(\mathbf{x},t)&=0.
\end{aligned} \tag{3}$$

The displacement vector $\mathbf{D}(\mathbf{x},t)$ is given by

$$\mathbf{D}(\mathbf{x},t)=\int_{-\infty}^{t}dt'\epsilon(t-t')\mathbf{E}(\mathbf{x},t'),$$

where $\epsilon(t-t')$ is the Fourier transform of $\epsilon(\omega)$, the local dielectric-response function appropriate for an isotropic and homogeneous medium. In the solution of these equations an arbitrary layer is denoted by p with $2\leq p\leq l$. The vacuum regions are denoted 1 and $l+1$, the latter representing the vacuum region occurring at the larger values of z.

After forming the wave equation for $\mathbf{E}$ from Eqs. (3) and Fourier-transforming in x, y, and t we find for the pth layer

$$(d^2/dz^2-\alpha_p{}^2)\mathbf{E}(z,\mathbf{k},\omega)=-\mathbf{S}_p(\alpha_p{}^2+\omega^2/v^2)\exp(i\omega z/v). \tag{4}$$

$\mathbf{S}_p$ is given by[8]

$$\mathbf{S}_p=-i\frac{4\pi e}{v}\frac{\mathbf{k}+\hat{z}\omega(1-\epsilon_p v^2/c^2)/v}{\epsilon_p(\alpha_p{}^2+\omega^2/v^2)}, \tag{5}$$

where $\mathbf{k}$ is a two-dimensional wave vector in the (x, y) plane given by $\mathbf{k}=k_x\hat{x}+k_y\hat{y}$, and $\alpha_p{}^2$ is given by

$$\alpha_p{}^2=k^2-\epsilon_p(\omega)\omega^2/c^2. \tag{6}$$

All of the Fourier transforms are defined by

$$f(x,y,z,t)=\int\frac{d\omega}{2\pi}\int\frac{dk_xdk_y}{(2\pi)^2}f(z,\mathbf{k},\omega)\exp(i\mathbf{k}\cdot\mathbf{x}-i\omega t). \tag{7}$$

The solution of Eq. (4) can be written as

$$\mathbf{E}_p(z,\mathbf{k},\omega)=\mathbf{F}_p\exp(\alpha_p z)+\mathbf{F}_p{}'\exp(-\alpha_p z)+\mathbf{S}_p\exp(i\omega z/v), \tag{8}$$

where $\mathbf{F}_p$ and $\mathbf{F}_p{}'$ are integration constants. However, if the divergence equations of (3) are applied to (8), one finds that there are only two independent integration constants. Indeed, because of cylindrical symmetry, the y components may be taken as zero. The x components are related to the z components by

$$F_p{}^x=(ik_x\alpha_p/k^2)F_p{}^z$$

and

$$(F_p{}^x)'=(-ik_x\alpha_p/k^2)(F_p{}^z)'. \tag{9}$$

The total number of constants which need to be determined is $2(l+1)$. These can be evaluated by using the continuity of $\epsilon_p E_p{}^z$ and $E_p{}^x$ at each interface between layers, in addition to the boundary conditions which must be applied to the solutions in the vacuum regions bounding the lamina. If $k^2>\omega^2/c^2$, the fields must decay exponentially as z goes to $\pm\infty$, which requires that

$$(F_1{}^z)'=F_{l+1}{}^z=0.$$

If $k^2<\omega^2/c^2$, this same pair of vacuum constants must be set equal to zero in order that the fields propagate only away from the lamina.

Applying the interface boundary conditions yields

$$\begin{aligned}F_{p+1}{}^z\exp(\alpha_{p+1}D_p)+(F_{p+1}{}^z)'\exp(-\alpha_{p+1}D_p)&=(\epsilon_p/\epsilon_{p+1})F_p{}^z\exp(\alpha_pD_p)\\&+(\epsilon_p/\epsilon_{p+1})(F_p{}^z)'\exp(-\alpha_pD_p)+[(\epsilon_p/\epsilon_{p+1})S_p{}^z-S_{p+1}{}^z]\exp[i(\omega/v)D_p]\end{aligned} \tag{10a}$$

and

$$\begin{aligned}F_{p+1}{}^z\exp(\alpha_{p+1}D_p)-(F_{p+1}{}^z)'\exp(-\alpha_{p+1}D_p)&=(\alpha_p/\alpha_{p+1})F_p{}^z\exp(\alpha_pD_p)\\&-(\alpha_p/\alpha_{p+1})(F_p{}^z)'\exp(-\alpha_pD_p)+[k^2(S_p{}^x-S_{p+1}{}^x)/ik_x\alpha_{p+1}]\exp[i(\omega/v)D_p],\end{aligned} \tag{10b}$$

where D_p is the value of the z coordinate for the pth interface (see Fig. 2). By using a vector-matrix formalism we can solve Eqs. (10) for the constants associated with layer $(p+1)$ in terms of those of layer p. Thus

$$\begin{bmatrix}F_{p+1}{}^z\exp\{[\alpha_{p+1}-i(\omega/v)]D_p\}\\(F_{p+1}{}^z)'\exp\{-[\alpha_{p+1}+i(\omega/v)]D_p\}\end{bmatrix}=M_p\begin{bmatrix}F_p{}^z\exp\{[\alpha_p-i(\omega/v)]D_{p-1}\}\\(F_p{}^z)'\exp\{-[\alpha_p+i(\omega/v)]D_{p-1}\}\end{bmatrix}+T_p, \tag{11}$$

where, with $m_p{}^\pm$ given by

$$m_p{}^\pm=\tfrac{1}{2}(\epsilon_p/\epsilon_{p+1}\pm\alpha_p/\alpha_{p+1}), \tag{12}$$

the 2×2 matrix M_p can be written as

$$M_p=\begin{bmatrix}m_p{}^+\exp\{[\alpha_p-i(\omega/v)]d_p\} & m_p{}^-\exp\{-[\alpha_p+i(\omega/v)]d_p\}\\m_p{}^-\exp\{[\alpha_p-i(\omega/v)]d_p\} & m_p{}^+\exp\{-[\alpha_p+i(\omega/v)]d_p\}\end{bmatrix}, \tag{13}$$

where d_p is the thickness of the pth layer. T_p, which contains the inhomogeneous parts of Eqs. (10), is given by

$$T_p=\begin{bmatrix} \dfrac{k/\alpha_{p+1}+i\omega(1-\epsilon_{p+1}v^2/c^2)/(vk)}{\epsilon_{p+1}(\alpha_{p+1}{}^2+\omega^2/v^2)}-\dfrac{k/\alpha_{p+1}+i\omega\epsilon_p(1-\epsilon_p v^2/c^2)/(vk\epsilon_{p+1})}{\epsilon_p(\alpha_p{}^2+\omega^2/v^2)} \\ \\ \dfrac{-k/\alpha_{p+1}+i\omega(1-\epsilon_{p+1}v^2/c^2)/(vk)}{\epsilon_{p+1}(\alpha_{p+1}{}^2+\omega^2/v^2)}+\dfrac{k/\alpha_{p+1}-i\omega\epsilon_p(1-\epsilon_p v^2/c^2)/(vk\epsilon_{p+1})}{\epsilon_p(\alpha_p{}^2+\omega^2/v^2)} \end{bmatrix}, \tag{14}$$

where

$$k=(k_x{}^2+k_y{}^2)^{1/2}.$$

Equation (11) is a recursion relation which, if repeatedly applied, will relate the "F" constants for the vacuum regions on the two sides of the slab. This allows the boundary conditions for the vacuum regions, previously described, to be applied. The resulting solution for the field constants $F_p{}^z$ and $(F_p{}^z)'$ can then be written as

$$\begin{bmatrix} F_{p+1}{}^z\exp\{[\alpha_{p+1}-i(\omega/v)]D_p\} \\ (F_{p+1}{}^z)'\exp\{-[\alpha_{p+1}+i(\omega/v)]D_p\} \end{bmatrix}=\prod_{i=1}^{p}(M_i)\begin{bmatrix} a \\ b \end{bmatrix}+\sum_{j=1}^{p}[\prod_{i=j+1}^{p}(M_i)]T_j, \tag{15}$$

using the notation that

$$\prod_{i=1}^{p}(M_i)$$

is the matrix product taken in the order $M_pM_{p-1}\cdots M_2M_1$. Defining the matrix N by

$$N=\begin{pmatrix} N_{11} & N_{12} \\ N_{21} & N_{22} \end{pmatrix}=\prod_{i=1}^{l}(M_i) \tag{16a}$$

and the vector $\mathbf{Q}$ by

$$\mathbf{Q}=\begin{pmatrix} Q_1 \\ Q_2 \end{pmatrix}=\sum_{j=1}^{l}[\prod_{i=j+1}^{l}(M_i)]T_j, \tag{16b}$$

we have for $k^2\neq\omega^2/c^2$

$$\begin{bmatrix} a \\ b \end{bmatrix}=\begin{bmatrix} Q_1/N_{11} \\ 0 \end{bmatrix}, \tag{17a}$$

which results from thinking of the vacuum regions as slightly absorbing such that the fields damp to zero as $|z|\to\infty$. At the same time, Eq. (17a) allows, when $k^2<\omega^2/c^2$, the resulting oscillatory fields to propagate only outwards. When $k^2=\omega^2/c^2$ we must have

$$\begin{bmatrix} a \\ b \end{bmatrix}=\begin{bmatrix} 0 \\ 0 \end{bmatrix}, \tag{17b}$$

in order that the fields be finite as $|z|\to\infty$.

Using Eqs. (8) and (15), the total electric field may be expressed. However, it is unnecessary to proceed in that manner. One can, at this point, calculate the total work done on the incident charge due to the electric field of the medium, $\mathbf{E}_M(\mathbf{x},t)$. $\mathbf{E}_M(\mathbf{x},t)$ is the total field minus the field which would exist if there were no material. The work done on the incident particle is

$$U=\int d^3x\int dt\,\mathbf{E}_M(\mathbf{x},t)\cdot\mathbf{J}(\mathbf{x},t). \tag{18}$$

If we Fourier-transform, we get for U the expression

$$U=-\int dk_xdk_y\int_{-\infty}^{+\infty}d\omega\,\Delta U(k,\omega), \tag{19}$$

where

$$\Delta U(k,\omega)=\frac{-1}{(2\pi)^3}\int_{-\infty}^{+\infty}dz\,\mathbf{E}_M(z,\mathbf{k},\omega)\cdot\mathbf{J}(z,-\mathbf{k},-\omega). \tag{20}$$

$[-\Delta U(k,\omega)]$ is the integrand of an integral which gives the entire energy change of a single electron passing through a lamina of dielectric material suspended in a vacuum. Thus, $\Delta U(k,\omega)$ represents that part of the energy

experimental energy-resolution function as described in Eq. (28).

Figure 7 shows $\langle\langle \Delta U(\Omega)\rangle\rangle$ for different sample thicknesses. Here a direct comparison is made between experiment and theory using a Gaussian energy-resolution function in the theoretical curves. Two half-widths for the Gaussian have been used, 0.017 and 0.010 eV. In each case the magnitudes of the peaks of the distributions have been made equal.

Consider the situation for a 700-Å film. The peak is due primarily to the principal peak in $\langle \Delta U(\Omega)\rangle$ shown in Fig. 5. The bulge on the high-frequency side of the peak in Fig. 7 is due to averaging over the structure on the high-frequency side of the main peak of Fig. 5 arising from the longitudinal optical mode and the large-K region of the low-frequency surface mode. Because of the asymmetry in the curve, it is seen that as the energy-resolution function widens, the main peak in $\langle\langle \Delta U(\Omega)\rangle\rangle$ will move to the right and at the same time the bulge will diminish. One sees from Fig. 7 that the experimental curves for 700 and 400 Å can be closely reproduced theoretically by picking the correct resolution function width. This does not appear to be the case, however, for the thinnest sample, as indicated by Fig. 7.

Some calculations were performed to check whether our results are sensitive to possible inaccuracies in the determination of the film thickness. Figure 8(a) shows the small effect on $\langle\langle \Delta U(\Omega)\rangle\rangle$ associated with increasing the thickness from 700 to 800 Å.

Little is known by the experimenters about the angular-response function except the geometrical stop angle of $(10)^{-4}$ rad. It is necessary, therefore, to investigate the possible changes in the energy-loss function caused by other plausible angular-response

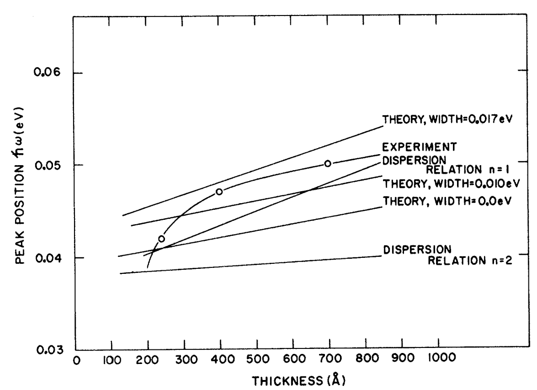

FIG. 6. Peak positions of the energy-loss distributions plotted against the thickness of the layer. The experiment is compared to three theoretical curves having different frequency-response function widths, but with the angular-response function always that of Eq. (29). [The theory curve for zero width is just $\langle \Delta U(\Omega)\rangle$.] Also shown is the position of peaks given by the dispersion relation if the angular distribution is assumed to be controlled by $K/(K^2+\Omega^2/\beta^2)^n$ for $n=1$ and $n=2$. Note the expanded ordinate scale.

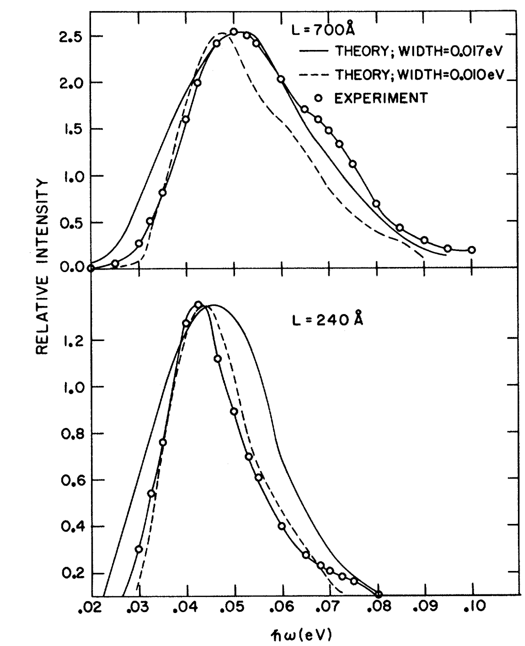

FIG. 7. Loss function $\langle\langle \Delta U(\Omega)\rangle\rangle$ with the angular-response function given by Eq. (29). Curves are for a Gaussian frequency-response function with widths of 0.017 and 0.010 eV. Separate graphs are shown for layer thicknesses of 240 and 700 Å. Also shown are the experimental curves of BGS.

functions. By extending the stop angle beyond $(10)^{-4}$ rad (or K beyond 430), we would expect the main peak of $\langle \Delta U(\Omega)\rangle$ in Fig. 5 to be unaffected. However, the two smaller peaks in the same figure should certainly grow in magnitude. This means that the bulge on the high-frequency side of $\langle\langle \Delta U(\Omega)\rangle\rangle$ shown in Fig. 7 should get larger. In Fig. 8(b) we have plotted the experimental loss function along with three theoretical loss functions. Each of the theoretical curves is for a thickness of 700 Å and a frequency response half-width of 0.010 eV, but each has a different angular-response function. Response function (I) is given by Eq. (29), and response function (II) is given by

$$\begin{aligned} f(K) &= 1, \qquad K<860 \\ &= 0, \qquad K>860. \end{aligned} \tag{30}$$

As the figure shows, the bulge does *not* increase significantly in relative size but the back side of the whole peak moves to larger frequencies. Also, the effect of a Gaussian function with half-width equal to 430 is plotted as function (III). From these curves it is apparent that the only way one could emphasize the bulge region of the distribution in relation to the main peak, would be to use a peculiar angular-response function which is lower for small angles than it is for large angles.

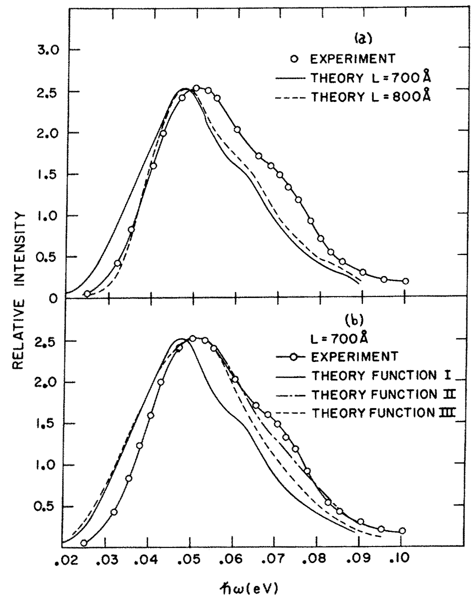

FIG. 8. (a) Loss function $\langle\langle\Delta U(\Omega)\rangle\rangle$ for two thicknesses, 700 and 800 Å, compared with the experimental results for a 700-Å film. The angular-response function is given by Eq. (29), and the frequency-response function is Gaussian with a half-width of 0.010 eV. (b) Loss function $\langle\langle\Delta U(\Omega)\rangle\rangle$ for three different angular-response functions, compared with the BGS experimental curve. All curves are for a thickness of 700 Å and all three theoretical curves were calculated using a Gaussian frequency-response function with a width of 0.010 eV. Angular-response function I is given by Eq. (29), II is given in Eq. (30), and III is a Gaussian centered at $K=0$ which has a half-width of 430.

LiF with Conducting Substrate

BGS[4] deposited their LiF films on a very thin layer of amorphous carbon. To investigate theoretically the possible effects of such a substrate, the problem of a layer of free-electron metal behind the LiF was considered. The metal was represented by a local dielectric function

$$\epsilon(\Omega)=1-[\Omega_p^2/\Omega(\Omega+i\gamma_m)], \tag{31}$$

where Ω_p is the plasma frequency of the metal in units of the LiF transverse optical frequency and γ_m is a damping parameter for the metal. In order to obtain the loss function when a good conductor is used as a substrate, constants appropriate to aluminum in the low-frequency region, $\hbar\omega_p=12.7$ eV and $1/\gamma_m=5.12(10)^{-15}\omega_t$ sec, were used.[16]

The electron energy-loss distribution $\Delta U(K,\Omega)$ with an aluminum backplate of 520- or 100-Å thickness is very different from ΔU with no backplate. The LiF low-frequency surface-mode peak is completely gone. All that appears is the LiF longitudinal optical mode at Ω_l and the low-frequency surface mode of Al.[17] Since the conductivity of the metal for $\Omega=1$ is approximately $2.6(10)^3\omega_t$, the electric field component parallel to the film face is suppressed at the metal-LiF interface. The polarization symmetry of the low-frequency surface mode in the LiF film thus precludes its occurring when a high-conductivity backplate of reasonable thickness is present.[18]

If a dielectric function is used which represents a metal with much lower conductivity, a larger electric field parallel to the surface at the metal-LiF interface could be sustained. To represent carbon, a dielectric function was used which had a plasma energy $\hbar\omega_p=0.1$ eV and a phenomenological relaxation time $1/\gamma_m=5(10)^{-13}\omega_t$ sec.[19] At the LiF transverse optical frequency, this "carbon" has a conductivity $\sigma(\omega_t)\sim2(10)^{-2}\omega_t$. Calculations were carried out for carbon layers of 520 and 100 Å on a 700-Å-thick LiF slab. The resulting distributions are essentially unchanged from the bare LiF distributions. Numerically, the peak of $\langle\langle\Delta U(\Omega)\rangle\rangle$ moves to higher energies by less than $(10)^{-3}$ eV. Perhaps this result is not unreasonable since this carbon has a conductivity equal to $(10)^{-5}$ of that of the Al.

What might be the effect on the distribution if we used another, somewhat higher conductivity, say $(10)^{-3}$ of Al, with the same carbon ω_p? Figure 9 shows that the conductivity is now high enough for the substrate modes to appear in the energy-loss function. We notice that the shape of the distribution has been affected and also that the bulge on the high-frequency side has *not* been emphasized. Now BGS subtracted the no-loss line shape from their data to obtain the loss function shown above. Thus it is possible that their subtraction could obscure structure arising from a backplate of moderate conductivity, since the structure occurs in the region where the subtraction is taking place. However, on the basis of our carbon results, it seems probable that the experimental results of BGS do not reflect backplate properties.

IV. DISCUSSION AND CONCLUSION

Using the local approximation, we have developed a theory for electron energy loss in films which includes the effects of retardation and substrates. We have

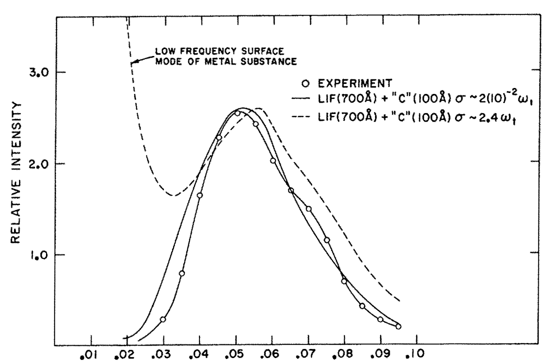

FIG. 9. Loss function $\langle\langle\Delta U(\Omega)\rangle\rangle$ showing the effect of moderately conductive "carbon." Shown for comparison is the experimental curve and the theory without substrate, which is the same as the theory with poorly conducting "carbon." All curves are for 700-Å LiF thickness and 100-Å "carbon" thickness.

shown that for very thin films of LiF (<1000 Å) retardation is not important in the energy range of the surface modes, but that for thicker films (~5000 Å) the changes that retardation makes in the surface-mode dispersion relations would possibly be observable in an energy-loss experiment. The most important reason for this is that the contribution of the high-frequency surface mode to the loss function is comparable to that of the low-frequency mode for films of larger thickness, and it is the high-frequency mode which changes most significantly when retardation is included.

The theory was applied to the case of thin films of LiF which have been studied experimentally by BGS[4] and for which FK[1] have worked out the normal-mode scheme. It was shown that because the half-width of the energy-response function of the experimental apparatus is of the same order of magnitude as the energy of the modes which are responsible for the energy loss, this response function must be considered if any detailed comparison with the data is to be made. It was found that the theoretical-loss function was relatively insensitive to the angular-response function of the apparatus and to small variations in the film thickness. The frequency-response function and a substrate, if present, can affect the loss function significantly.

All of the parameters concerning the experiment on the single LiF film were adjusted to attempt to match two characteristics of the experimental distribution: the peak position and the bulge on the high-frequency side of the peak. From our results these characteristics can be readily interpreted physically. The principal peak arises from the small wave-vector portion of the low-frequency surface-mode dispersion curve and the bulge from the large wave-vector portion of this same dispersion curve. This means the bulge occurs where $\epsilon(\Omega)\cong-1$, independent of film thickness. The peak and the bulge obtained experimentally could not simultaneously be reproduced in complete detail, but the structure of the theoretical curves is in excellent agreement with the experimental results.[20]

Calculations showed that if the LiF film is deposited on a low-conductivity free-electron backplate [conductivity $\sim(10)^{-5}$ of that of Al at $\omega=\omega_t$], there is a negligible change in the loss distribution from the distribution with no substrate. For higher conductivities the surface modes of that particular "metal" appear in the loss distribution.

There seems to be no doubt that the general features of the loss experiment of BGS are described well by the local theory. However, the lack of knowledge about the exact frequency- and angular-response functions, and the dielectric function of the substrate negates any chance of obtaining any more theoretical information from their data. There are several ways of increasing the amount of information which can be obtained from this kind of an experiment. One might try thicker films. If one can successfully eliminate effects associated with multiple scattering, then data on the high-frequency surface mode would result leading to information on retardation effects. Experimentally, an improvement in the angular resolution by a factor of 4 or an improvement in the energy resolution by a factor of even 2 would be highly significant. Such improvements might well provide an answer to the question as to whether a nonlocal theory is really necessary to understand the physical processes in this kind of thin film.

In analyzing their data, BGS plotted the energy of the peak of the experimental loss distribution as a function of the slab thickness. BGS then compared this plot with a theoretical curve derived from the dispersion curves of FK. This theoretical curve was obtained by intersecting the FK dispersion curves for various slab thicknesses with the curve made of the maxima of the angular distribution

$$\frac{K}{K^2+\Omega^2/\beta^2}, \tag{32}$$

where $\beta=v/c$. These intersection points are assumed to yield values of Ω for which the distribution $\langle\Delta U(\Omega)\rangle$ has its peak. Equation (32) and also the angular distribution

$$\frac{K}{(K^2+\Omega^2/\beta^2)^2} \tag{33}$$

appear as coefficients of the bulk and surface terms, respectively, of Eq. (23) of the nonretarded theory given by Ritchie.[3] For purposes of clarification, Fig. 6 shows plots of peak position versus thickness obtained (1) theoretically from both of the above angular distributions, (2) from the complete theory for three resolution functions, 0.017, 0.010, and 0.0 eV [$=\langle\Delta U(\Omega)\rangle$], and (3) from the BGS experiment. Noting the expanded ordinate in Fig. 6, we see that, as BGS stated in their report, the curve obtained directly from the dispersion relation gives a sufficiently close comparison to the data to suggest the basic validity of the local theory. However, we have shown in this paper that to understand the experimental results in any detail requires considerably more than a knowledge of the dispersion curves.

---

* Work performed in the Ames Laboratory of the U.S. Atomic Energy Commission, contribution No. 2673.

[1] R. Fuchs and K. L. Kliewer, Phys. Rev. **140**, A2076 (1965); **144**, A495 (1966); **150**, 573 (1966). Hereafter to be referred to collectively as FK.

[2] E. Kröger, Z. Physik **216**, 115 (1968).

[3] R. H. Ritchie, Phys. Rev. **106**, 874 (1957); H. Raether, Ergeb. Exakt. Naturw. **38**, 84 (1965). See also Ref. 11 for a theory including retardation for bulk materials.

[4] H. Boersch, J. Geiger, and W. Stickel, Phys. Rev. Letters **17**, 379 (1966), hereafter to be referred to as BGS.

[5] T. Fujiwara, and K. Ohtaka, J. Phys. Soc. Japan **24**, 1326 (1968), hereafter to be referred to as FO.

[6] The treatment here parallels that of Kröger for the case of one slab. See. Ref. 2.

[7] The light line is the line $\Omega=K$.

[8] Compare with Eq. (14) of Ref. 2.

[9] No reciprocal-lattice vectors appear here in this small-wave-

vector approximation. Because the momentum transferred in the plane of the slab is small, we need not take the wave vector into account for the components of the dynamical matrix of nonzero reciprocal-lattice vector. These components, independent of the transfer wave vector, have been summed and appear as the Lorentz-local-field correction which is contained in the dielectric function used. See Ref. 1.

[10] See Eq. (12) of Ref. 2.

[11] C. Von Festenberg and E. Kröger, Phys. Letters **26A**, 339 (1968).

[12] J. R. Jasperse, A. Kahan, and J. N. Plendl, Phys. Rev. **146**, 526 (1966).

[13] J. Geiger (private communication).

[14] $K=430$ is equivalent to a scattering angle of $(10)^{-4}$ rad.

[15] Recently Lucas and Kartheuser [Phys. Rev. B **1**, 3588 (1970)] have developed a single slab nonretarded theory for $\langle \Delta U(\Omega) \rangle$ which gives results comparable to those of FO except in the frequency range near $\Omega=\Omega_l$. Lucas and Kartheuser neglected the interaction between the bulk modes and the surface modes and this interaction gives rise to significant effects near $\Omega=\Omega_l$.

[16] H. Ehrenreich, H. R. Phillipp, and B. Segall, Phys. Rev. **132**, 1918 (1963).

[17] For details of the Al loss distribution see Ref. 2.

[18] See also the first paper of Ref. 1, p. A2084.

[19] The plasma energy chosen is the lowest energy at which the real part of the dielectric function of graphite has a zero according to the data of H. R. Philipp [*Optical Properties and Electronic Structure of Metals and Alloys* (North-Holland, Amsterdam, 1966), p. 408]. We calculated the relaxation time using the carbon conductivity at zero frequency given in the *Handbook of Chemistry and Physics*, 48th ed. (Chemical Rubber Publishing Co., Akron, 1968) p. f-132.

[20] H. Boersch, J. Geiger, and W. Stickel [Z. Physik **212**, 130 (1968)] show theoretical energy-loss curves which clearly include both angular- and energy-resolution functions. Their Figs. 5 and 6 are much like our Figs. 7 and 6. However, this paper of Boersch, Geiger, and Stickel contains almost no details concerning their treatment.

PHYSICAL REVIEW B VOLUME 2, NUMBER 11 1 DECEMBER 1970

Electronic-Structure Studies of Solids. I. Fourier Representation Method for Madelung Sums*

FRANK E. HARRIS AND HENDRIK J. MONKHORST

Department of Physics, University of Utah, Salt Lake City, Utah 84112

(Received 29 October 1969)

By use of Fourier-integral representations and lattice orthogonality relations, Madelung sums are cast in a form which explicitly separates contributions due to crystal symmetry from those due to the detailed arrangement of neighboring ions. The usefulness and mathematical soundness of the method are demonstrated by verifying known Madelung constants and by obtaining more accurate values for the electrostatic energies of low-density plasma models. The method is also easily applied to the study of ionic displacements or crystal defects.

I. INTRODUCTION

In connection with electronic-structure calculations of crystalline solids, we found it convenient to introduce a Fourier-integral representation for the electrostatic potential energy. The various contributions of opposite sign exhibit cancellations and limiting properties also manifested by classical electrostatic interactions as encountered in the evaluation of Madelung constants. We therefore found it profitable to reinvestigate the Madelung problem to establish the correctness of the mathematical steps, and to determine highly accurate values of numerical constants entering the electronic-structure studies.

The classical methods for the evaluation of Madelung sums are those of Evjen[1] and Ewald.[2] These sums, which are conditionally (and slowly) convergent, are in Evjen's method analyzed by grouping contributions into shells with vanishing low-order multiple moments. Ewald introduces an integral transformation which is then broken into two parts, each of which is more rapidly convergent than the original sum. However, neither of these methods has really made the evaluation of Madelung sums as simple as might be desired. Refinements and modifications of the Evjen and Ewald procedures have therefore been investigated; of note are the contributions of Emersleben[3] and of Bertaut.[4]

The explicit use of Fourier transforms in lattice-sum evaluations has been considered before,[5] and in fact a treatment containing some of the features of that described here is to be found in the work of Nijboer and De Wette.[6] However, the previous use of Fourier methods has been such as to avoid the mathematical difficulties associated with arrays of point charges, and the finally resulting formulations are not optimal for the application we contemplate to quantum mechanics. In contrast, we find that passage to the point-charge limit leads to simple and useful final formulas.

Our final formulas in effect calculate the electrostatic energy as a deviation from a limiting case in which ions of one sign are immersed in a uniform background of opposite charge. This limiting case, familiar in plasma physics, is treated with the aid of the Euler-Maclaurin summation formula. The notion of a point-charge array and compensating uniform background has also entered previous discussions of Madelung energies. For example, Tosi[7] reviews methods whereby this idea can be used to relate Madelung constants of different structures of the same lattice symmetry. The resulting formulas are similar to those presented here. The most